Received 19 September 2023; revised 24 October 2023; accepted 7 November 2023. Date of publication 13 November 2023; date of current version 6 December 2023. The review of this article was arranged by Editor T. Narita.

Digital Object Identifier 10.1109/JEDS.2023.3332094

Use of Nanosecond Laser Annealing for Thermally Stable Ni(GeSn) Alloys

ANDREA QUINTERO, PABLO ACOSTA ALBA, JEAN-MICHEL HARTMANN, DAVID COOPER, PATRICE GERGAUD, VINCENT REBOUD, AND PHILIPPE RODRIGUEZ (Member, IEEE)

Univ. Grenoble Alpes, CEA, LETI, 38000 Grenoble, France

CORRESPONDING AUTHOR: P. RODRIGUEZ (e-mail: philippe.rodriguez@cea.fr)

This work was supported in part by the French National Research Agency (ANR) through the "Investissements d'avenir" Programs under Grant ANR 10-AIRT-0005 (IRT NANOELEC) and Grant ANR 10-EQPX-0030 (EQUIPEX FDSOI 11); in part by the CEA DSM/DRT Phare Project "Photonics"; in part by the CARNOT Project EDEN; and in part by the European Union's Horizon 2020 LASTSTEP Project under Grant Agreement 101070208.

ABSTRACT In this study, we have conclusively used UV-nanosecond laser annealing (UV-NLA) as an alternative to classical rapid thermal annealing (RTA) for the formation of stable Ni-GeSn alloys. The phase formation sequence was similar to the one obtained with RTA. At low laser energy densities (ED) and after the consumption of Ni, the Ni-rich phase, $Ni_5(GeSn)_3$, was first obtained. This phase was followed, for higher ED, by the mono-stanogermanide phase Ni(GeSn). Surface wrinkles appeared at high ED, resulting in a sheet resistance (R_{sh}) increase. Meanwhile, R_{sh} variations were mainly governed by the phases that were present at lower ED. By combining various analyses, we did not see any Ni(GeSn) agglomeration or Sn segregation. The use of UV-NLA yielded thermally stable Ni(GeSn) contact layers.

INDEX TERMS GeSn, NiGeSn, laser annealing, contact.

I. INTRODUCTION

Germanium-tin alloys have shown very promising properties for microelectronics and Si-based photonics applications. As far as complementary metal-oxide-semiconductor (CMOS) technologies are concerned, GeSn can be used as high-mobility channel or as source and drain stressor [1], [2], [3], [4]. Since the first demonstration of an optically pumped direct-bandgap GeSn laser in 2015 [5], the interest of using GeSn for Si-based photonics has not slowed down [6]. Innovative Mid Infra-Red (MIR) GeSn-based devices such as Light Emitting Diodes (LEDs) [7], photo-detectors [8], electrically pumped lasers at low temperature [9] and optically pumped lasers at room-temperature have thus been reported [10], [11], [12].

Despite the growing interest in GeSn alloys, challenges that need to be overcome include the growth of high crystalline quality GeSn layers on Si and Ge substrates with relatively high Sn contents [13]. The quest for high crystalline quality GeSn layers is indeed an incessant fight against thermodynamics and physical properties. First, there are large lattice parameters mismatches between Sn and Ge or Si, 14.7% and 19.5%, respectively [14]. Critical thicknesses for plastic relaxation, e.g., thicknesses above which misfit dislocations would start to happen, are thus low when growing GeSn on Ge and a few nanometers only for GeSn on Si. Another challenge is that, at thermal equilibrium, the solid solubility of Sn in Ge is as low as 1 at.% below 500 °C [15]. Looking at the Ge–Sn binary diagram, the eutectic temperature for the binary alloy is as low as 231.1 °C [16]. These two properties strongly favor Sn precipitation/segregation in the Ge–Sn system. As a consequence, the use of low temperature, non equilibrium processes, is mandatory to obtain high crystalline quality GeSn layers [13].

Whatever the final application, high quality contacts are needed to obtain microelectronics or photonics devices with required performances. Ni-based metallization is the most reported strategy on GeSn [17]. Ni has indeed the benefit of forming a Ni(GeSn) alloy at relatively low temperature [18] with low resistivity and contact resistance [1], [19]. On the other hand, the main drawback of the Ni/GeSn system is its poor thermal stability because

© 2023 The Authors. This work is licensed under a Creative Commons Attribution-NonCommercial-NoDerivatives 4.0 License.
For more information, see https://creativecommons.org/licenses/by-nc-nd/4.0/

of two phenomena: Ni(GeSn) agglomeration and Sn segregation [20]. Technological options have thus been assessed to enhance the thermal stability of the Ni/GeSn system. One can indeed play with various technological levers, from GeSn surface engineering to metallization. For instance, Wang et al. used Pt co-sputtering [21], while Wan et al. added a Pt interlayer [22]. In our group, we evaluated various alloying elements, such as Pt and Co [23], [24]. The use of pre-amorphization by implantation (PAI) prior to metallization was also assessed [25], [26] and an alternative metallization with Ti was explored [27], [28]. Generally, Ni(GeSn) alloys were grown using rapid thermal annealing (RTA). The thermal stability of the Ni/GeSn system can also be improved with alternative annealing processes. Microwave annealing (MWA) [29] and laser thermal annealing (LTA) [30], [31], [32] were recently assessed to reduce the thermal budget. Although the capacity of LTA treatments of obtaining low resistance Ni-based contacts on GeSn was confirmed, studies have also demonstrated the formation of Sn-rich vertical columns or filaments during the liquid-solid regrowth mechanisms governing layer formation [30], [31].

Apart from the formation of Ni(GeSn) alloys, laser annealing processes have mainly been employed to tailor and enhance the crystalline quality (grain growth, crystallization and so on) of GeSn layers during, or after, their low thermal budget growth [33], [34], [35], [36], [37]. Laser annealing was also used to reverse the stress in GeSn layers [36] or to modulate photodiode optoelectronic properties by Sn atoms redistribution [38].

This study aims to assess the ability of UV-nanosecond laser annealing (UV-NLA) to fabricate thermally stable Ni(GeSn) alloys. We first use X-ray diffraction (XRD) measurements to analyze the phase formation sequence. We then investigate the surface and cross-sectional properties of the Ni-based contact layers using various characterization methods. Finally, we evaluate the electrical properties of the contacts as a function of laser energy density by measuring the sheet resistance. Our results show that UV-NLA is a promising technological approach to fabricate Ni-based contact layers on GeSn with good thermal stability.

II. EXPERIMENTAL

We epitaxially grew 60 nm-thick high quality GeSn layers with 10 at.% of Sn in substitutional sites at 325 °C on Ge-buffered Si (100) substrates in a reduced pressure chemical vapor deposition (RPCVD) tool [39]. After the GeSn surface preparation (wet cleaning and/or in-situ plasma treatment to remove native oxide), we deposited 10 nm thick Ni layers capped with 7 nm thick TiN layers using room temperature magnetron sputtering. We used classical Ar-based plasma sputtering to deposit the Ni layers at 65 mTorr, and reactive sputtering using N_2 to deposit the TiN layers at 35 mTorr. A schematics of the resulting stacks is shown in Fig. 1(a). Then, we performed UV-nanosecond laser annealing (UV-NLA) on samples using a SCREEN-LT3100 tool based on

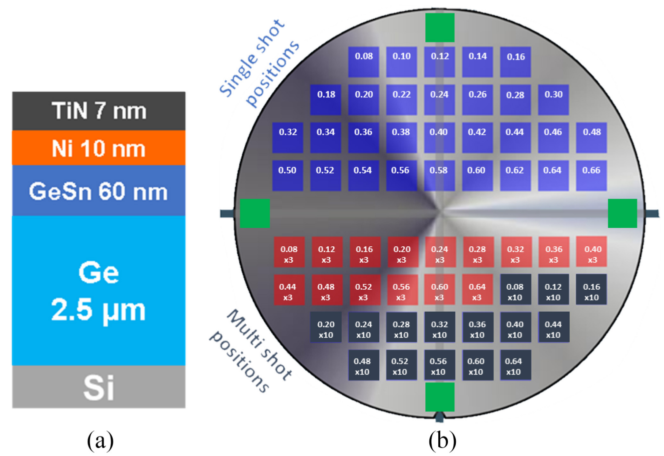

FIGURE 1. (a) Schematics of samples used in this study and (b) map of UV-NLA conditions probed on the wafer surface.

a XeCl excimer laser (308 nm wavelength) with a pulse duration of 160 ns ± 2 ns (Full Width at Half Maximum). 15 × 15 mm^2 fields were irradiated with laser Energy Densities (ED) ranging from 0.08 up to 0.66 J/cm^2 with 0.02 J/cm^2 steps. We used single and cumulative pulses (3 and 10 pulses) with various laser conditions on the 69 positions specified in Fig. 1(b).

To characterize the impact of UV-NLA in terms of phase sequence evolution, we performed X-Ray Diffraction (XRD) analyses using a X'Pert Pro PANalytical X-ray diffractometer. We also carried out Atomic Force Microscopy (AFM) using a Bruker FastScan equipment, Scanning Electron Microscopy (SEM), STEM HAADF (Scanning Transmission Electron Microscopy with High-Angle Annular Dark Field detector) coupled with EDX (Energy Dispersive X-ray) to assess the morphological properties. Finally, we used a four-point probe meter to achieve sheet-resistance (R_{sh}) measurements and characterize the electrical properties.

III. EVALUATION OF THERMAL REGIMES

We experimentally determined thermal regimes and melt threshold using in-situ time-resolved reflectivity (TRR) measurements. For samples treated with a single laser pulse, the surface reflectivity evolution as a function of time was recorded for each laser shot at various energy densities (ED). All profiles were then gathered to obtain the color map shown in Fig. 2.

TRR intensity variations are related to morphological or structural property changes. We were thus able to experimentally determine the melt threshold based on Fig. 2 analysis. The black dashed line shows that ED threshold for $TiN/Ni/Ge_{0.9}Sn_{0.1}$ samples. We observed an intensity decrease at around 200 ns for ED $>$ 0.36 J/cm^2 and more clearly for ED $>$ 0.40 J/cm^2. The melt threshold of this system was thus in this ED range.

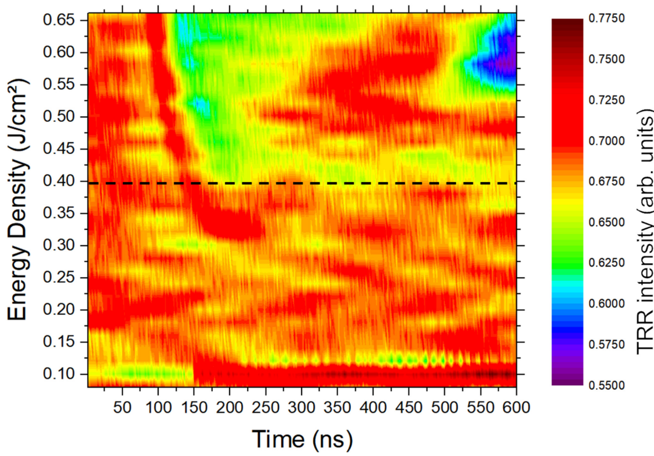

FIGURE 2. Time-Resolved Reflectometry (TRR) for various energy densities during the laser annealing of TiN/Ni/$Ge_{0.9}Sn_{0.1}$ samples.

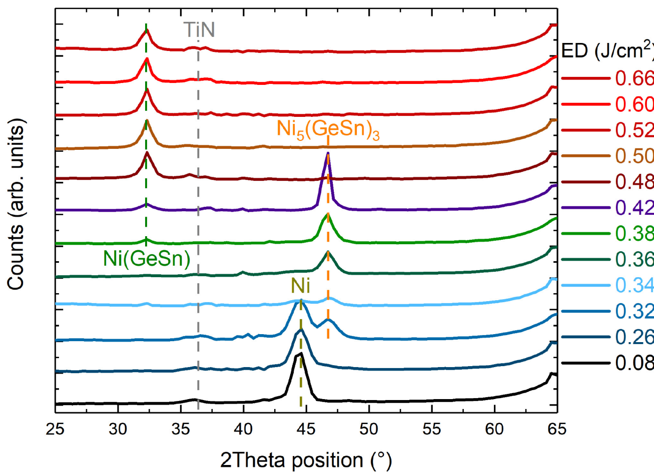

FIGURE 3. XRD patterns obtained for Ni/$Ge_{0.9}Sn_{0.1}$ samples annealed by UV-NLA using a single laser pulse at various energy densities.

IV. RESULTS AND DISCUSSION

A. STUDY OF PHASE FORMATION SEQUENCE

One of the aims of annealing a metal-semiconductor system is to promote its evolution towards a more stable thermodynamic state. Diffusion and nucleation mechanisms come into play during an annealing, resulting in the formation of intermetallic phases. As far as the Ni/GeSn system is concerned, the mono-stanogermanide Ni(GeSn) phase corresponds to the less resistive phase and therefore the most suitable for contacting GeSn-based devices [17]. For this reason, it is of utmost importance to verify the impact of UV-NLA on the phase formation sequence and its ability to form the desired phase. We have thus analyzed the phase formation evolution for the Ni/$Ge_{0.9}Sn_{0.1}$ system as a function of UV-NLA energy density using $\theta - 2\theta$ XRD scans. Corresponding patterns are shown in Fig. 3.

For all energy densities (ED), we can observe a broad TiN 111 diffraction peak with a weak intensity at around 36.4°. At low ED in the 0.08 – 0.32 J/cm^2 range, there is an intense

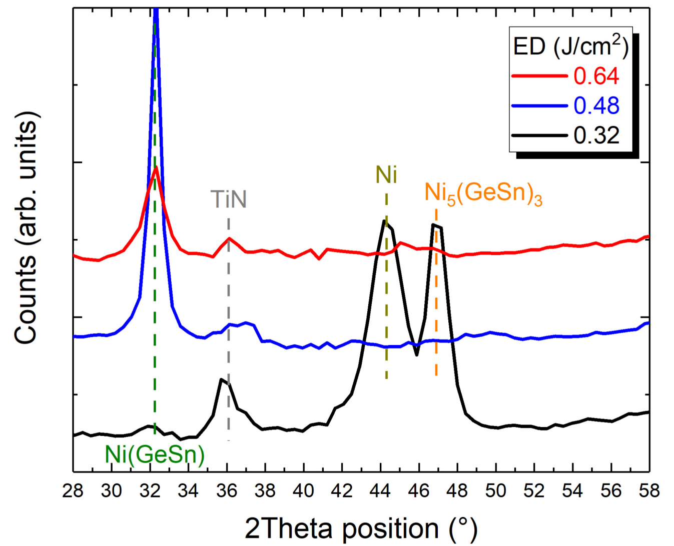

FIGURE 4. XRD patterns obtained for Ni/$Ge_{0.9}Sn_{0.1}$ samples annealed by UV-NLA using 10 cumulative laser pulses at 0.32, 0.48 and 0.64 J/cm^2.

diffraction peak at around 44.6° due to the Ni 111 diffraction line. From an energy density threshold of 0.32 J/cm^2 and up to 0.42 J/cm^2, there is a diffraction peak around 46.7°. Based on our previous studies, this peak has been attributed to the Ni-rich phase, namely the ϵ-$Ni_5(GeSn)_3$ hexagonal structure [40] – it corresponds to the 110 diffraction line.

At higher energy densities, namely above 0.38 J/cm^2, a new diffraction peak appears around 32.3°. According to our former investigations [40], this peak corresponds to the mono-stanogermanide phase Ni(GeSn), 200 diffraction line, and is present up to the highest ED probed. In addition, the angular position of the Ni(GeSn) diffraction line is always at 32.3° for ED ranging from 0.38 up to 0.66 J/cm^2, i.e., we do not observe any 2θ variation of this peak with increasing ED. Such a behavior is likely due to a lack of composition change in this ED range for the Ni(GeSn) phase. The use of UV-NLA might also modify the Ni(GeSn) texture as only one out-of-plane diffraction line related to this phase is observed on laser annealed samples at 32.3°. Meanwhile, multiple Ni(GeSn) diffraction lines were observed on the XRD patterns of RTA annealed samples [23], [40]. The related discussion is however out of scope of the current study.

We have then studied the impact of performing cumulative laser pulses on the phase sequence. Fig. 4 shows XRD patterns for Ni/$Ge_{0.9}Sn_{0.1}$ samples annealed by UV-NLA using 10 cumulative laser pulses at energy densities of 0.32, 0.48 and 0.64 J/cm^2.

We have demonstrated the same phases as for single laser pulses. The energy densities at which they appear are modified however. For the lowest energy density studied (0.32 J/cm^2), Ni coexists with $Ni_5(GeSn)_3$ and also with Ni(GeSn) as shown by the broad peak with a weak intensity around 32.3°. At higher ED, the only visible peak (in addition to the TiN one) is from Ni(GeSn).

Compared to RTA processes [17], the use of UV-NLA results in a similar phase formation sequence with (i) the consumption of Ni and the formation of a Ni-rich $Ni_5(GeSn)_3$ phase at low energy densities (i.e., low thermal budgets) and (ii) the consumption of the Ni-rich phase together with the formation of the mono-stanogermanide phase Ni(GeSn) at higher energy densities (i.e., high thermal budgets). Whatever the annealing procedure involved such as single or cumulative pulses, we do not have any diffraction lines associated with the presence of β-Sn when using UV-NLA, which is unlike RTA processes [17]. In addition, as described previously, the angular position of the diffraction line related to the Ni(GeSn) phase is fixed for the ED range probed. In previous studies, the variation of the angular position 2θ of the diffraction line of the Ni(GeSn) phase was used to highlight the Sn out-diffusion [41], [42]. With UV-NLA, no Sn segregation is thus observed by XRD (i.e., at least no long-range Sn diffusion). The very short process duration of laser annealing compared to RTA, in combination to the melting state in which reactions occur, may have had an impact on diffusion and kinetics in the Ni/GeSn system. This process could prevent Sn segregation, which could be a major step towards the formation of thermally stable contacts on GeSn.

B. MORPHOLOGICAL EVOLUTION

We have performed Atomic Force Microscopy (AFM) measurements to characterize the surface morphology of $Ni/Ge_{0.9}Sn_{0.1}$ samples and its evolution with the UV-NLA energy density. Fig. 5 shows AFM images, with a scan size of 5 μm × 5 μm, obtained for samples annealed at various EDs.

At low ED and up to 0.32 J/cm^2, samples show a cross-hatch pattern along the $\langle 1\,1\,0\rangle$ crystallographic directions. Such a specific morphology is due to the epitaxy of GeSn layers on the Ge virtual substrates underneath [39], [43]. Low ED laser pulses do not modify the original surface morphology. At higher ED, the surface roughness increases from about 1 nm up to about 10 nm (exact RMS values are given in Fig. 5) and the surface morphology drastically changes. This morphology change occurs more or less at the melting threshold of the system, as detailed in Section III.

The deterioration of the surface morphology is due to the formation of wrinkles on the sample's surface. Wrinkles appearance is related to a stress relaxation of the TiN capping layer, this layer having a compressive stress of about –6 GPa (We calculated the TiN film stress from wafer bow measurements before and after TiN deposition). When the GeSn underneath layer reaches the melting threshold, the stress of the TiN layer is released through deformation by wrinkles formation [44]. This unwanted phenomenon is relatively well known. It can be suppressed or, at least, mitigated by stress reduction coming from the TiN capping layer or by patterning the structure.

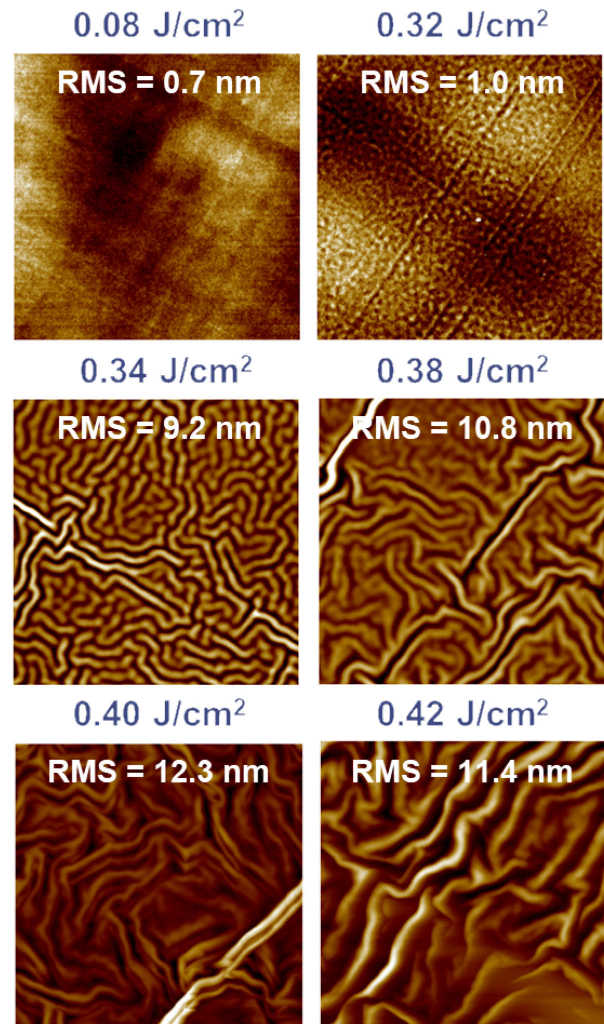

FIGURE 5. **AFM images (scan size: 5 μm × 5 μm) of $Ni/Ge_{0.9}Sn_{0.1}$ samples annealed by UV-NLA at various energy densities. AFM image sides are more or less oriented along the $\langle 1\,0\,0\rangle$ directions.**

The surface morphology of UV-NLA samples is mainly governed by the formation of wrinkles at high ED. Meanwhile, for RTA samples annealed at temperatures greater than or equal to 350 °C [24], [45], it was mostly controlled by Ni(GeSn) agglomeration and Sn segregation.

We have further characterized wrinkle formation with top view SEM (see Fig. 6). In particular we have investigated the impact of energy density and number of laser pulses on the number and amplitude of wrinkles.

At 0.32 J/cm^2, there are no wrinkles on the sample's surface whatever the number of laser pulses. We have the formation of wrinkles for EDs greater than or equal to 0.34 J/cm^2 with a single laser pulse – in good agreement with the AFM results shown in Fig. 5 – confirming that the melting threshold is reached. In general, wrinkle patterns have three evolution stages: initial growth, coarsening then equilibration. Wrinkles gradually increase and saturate in terms of wavelength and amplitude, with in the end, the

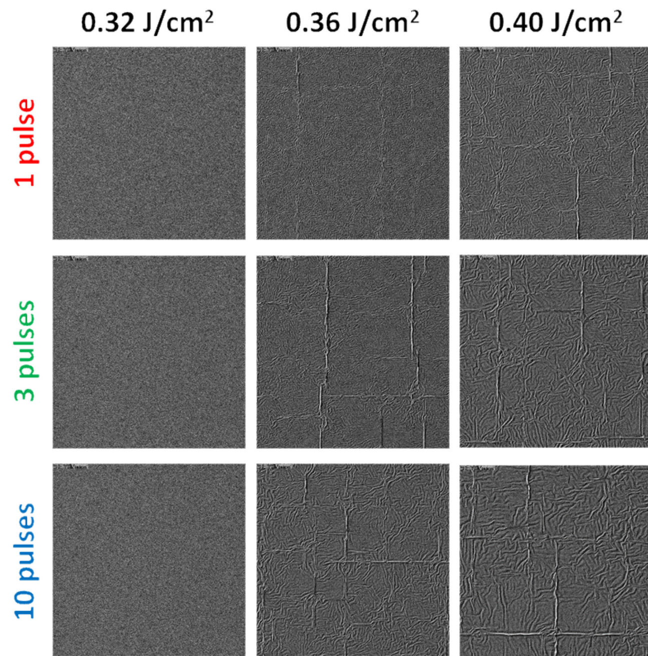

FIGURE 6. Top view SEM images (scan size: 30 μm × 30 μm) of $Ni/Ge_{0.9}Sn_{0.1}$ samples annealed by UV-NLA with 1 laser pulse (top row), 3 laser pulses (middle row) and 10 laser pulses (bottom row) at 0.32, 0.36 and 0.40 J/cm^2. Image sides are oriented along the ⟨1 1 0⟩ directions, i.e., at 45° to the directions in Fig. 5.

formation of equilibrium wrinkle patterns [46]. In our case, the number and amplitude of wrinkles increase with (i) the energy density and (ii) for a given ED, the number of laser pulses, as shown in Fig. 6.

We have also used cross-sectional STEM HAADF observations coupled with EDX measurements to characterize the morphology and elemental distribution in $Ni/Ge_{0.9}Sn_{0.1}$ samples annealed by UV-NLA. Fig. 7 shows STEM HAADF images and corresponding EDX mappings of a sample annealed by UV-NLA with 1 laser pulse at 0.52 J/cm^2.

Wrinkles are present in Fig. 7 STEM HAADF image, namely the morphology previously observed by AFM and top view SEM observations at high ED. Despite the high amplitude observed, the TiN capping layer is still continuous and follows the wrinkle's wave shape as shown by the Ti EDX mapping. Using the STEM HAADF image, we can estimate the TiN length variation, after UV-NLA annealing, at about 1%. This length variation range is in good agreement with the total in-plane strain relaxation for a layer with an initial stress of about –6 GPa.

Ge, Sn and Ni EDX maps show that the Ni(GeSn) composition is quite homogeneous without any evidence of Sn segregation or NiGe agglomeration as previously reported for RTA annealed samples [47], [48]. The use of UV-NLA is thus clearly beneficial to eliminate, or at least minimize, these unwanted phenomena and promote thermally stable Ni(GeSn) alloys.

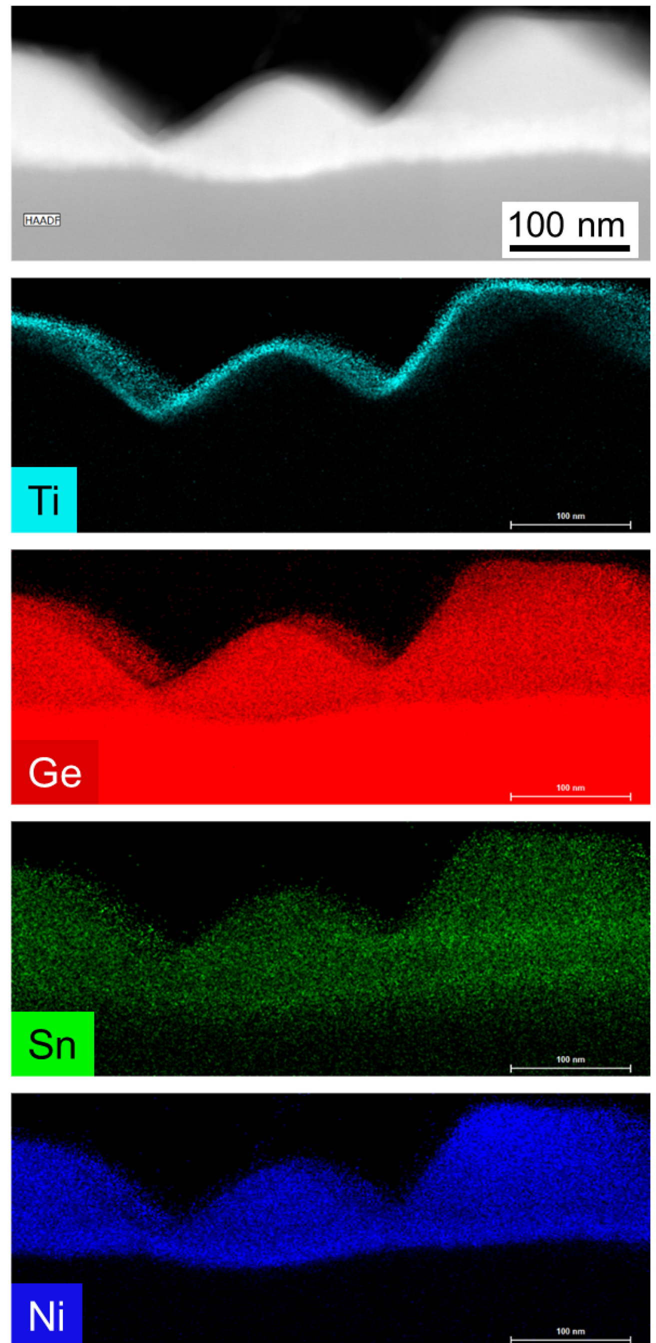

FIGURE 7. STEM HAADF images and corresponding EDX maps of a $Ni/Ge_{0.9}Sn_{0.1}$ sample annealed by UV-NLA with 1 laser pulse at 0.52 J/cm^2.

C. ELECTRICAL PROPERTIES EVOLUTION

Finally, we have measured the evolution of the electrical properties of the $Ni/Ge_{0.9}Sn_{0.1}$ system as a function of energy densities using sheet resistance (R_{sh}) measurements. The results are shown in Fig. 8.

At low energy densities, R_{sh} remains constant at around 28-29 Ω/sq. For ED between 0.32 and 0.36 J/cm^2, R_{sh} slightly increases up to 33 Ω/sq, as shown in Fig. 8 with, as an overlay, the phases in presence for each ED based

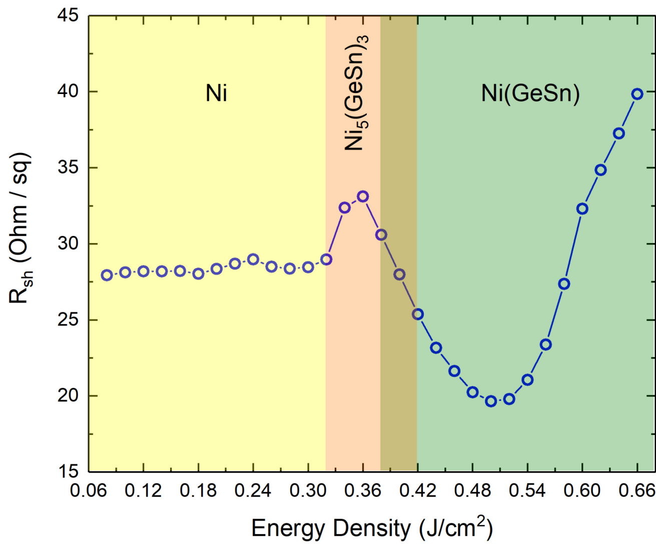

FIGURE 8. Sheet resistance (R_{sh}) evolution with the Energy Density (from 0.08 up to 0.66 J/cm^2) for Ni/ $Ge_{0.9}Sn_{0.1}$ samples annealed by UV-NLA with a single laser pulse.

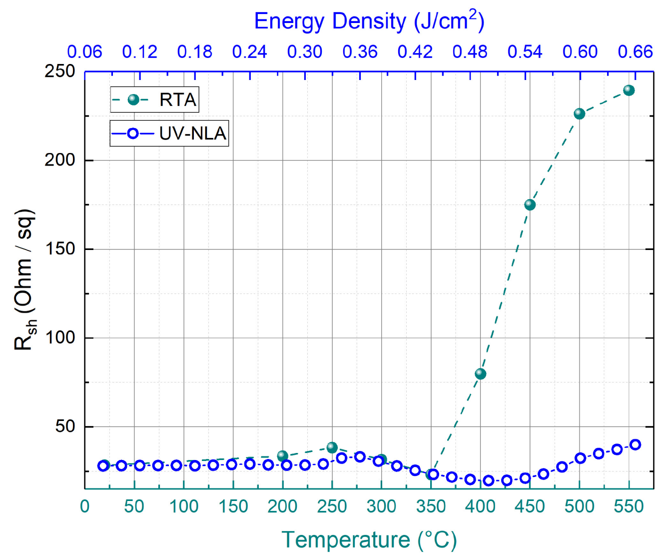

FIGURE 9. Comparison of sheet resistance (R_{sh}) evolution for $Ni/Ge_{0.9}Sn_{0.1}$ samples annealed by UV-NLA with a single laser pulse (open circles) and by RTA for 30 s in a N_2 environment (closed spheres).

on Fig. 3 XRD patterns. This R_{sh} increase is thus due to the consumption of Ni and the growth of the Ni-rich phase $Ni_5(GeSn)_3$. Then, for ED higher than 0.36 J/cm^2, R_{sh} progressively decreases reaching 19.7 Ω/sq at 0.5 J/cm^2. This decrease occurs simultaneously with the consumption of the Ni-rich phase and the formation of the less resistive Ni(GeSn) phase. For ED above 0.5 J/cm^2, R_{sh} moderately increases to reach about 40 Ω/sq at 0.66 J/cm^2. This increase could be due to wrinkling and thus higher surface roughness. The roughness (surface or interface roughness) induces electron scattering and thus degrades the electrical properties: resistivity increase or higher ρ_c have been reported for metals [49] or silicides [50]. This assertion has been consolidated by the analysis of sheet resistance measurements performed on samples with 3 or 10 cumulative laser pulses. At low ED, R_{sh} values and overall behavior are similar to that with a single laser pulse. At higher ED, the R_{sh} values increase more rapidly, reaching 52 and 58 Ω/sq for samples with 3 or 10 cumulative laser pulses, respectively. As shown in Fig. 6, this behavior could be due to the increase of the number and amplitude of wrinkles with the number of laser pulses.

Fig. 9 shows a comparison between sheet resistances for samples annealed by UV-NLA or RTA (30 s in a N_2 environment) [17], [24]. Compared to RTA, the R_{sh} increase observed with UV-NLA is very low. We indeed have R_{sh} values reaching 250 Ω/sq for samples annealed at high temperature by RTA. Meanwhile, the highest R_{sh} values obtained with UV-NLA over the ED range probed do not exceed 50 Ω/sq. Using UV-NLA we also achieve a larger suitable process window whereas it is quite narrow with RTA (mainly centered around 350 °C). We also obtain slightly lower R_{sh} values for UV-NLA. As mentioned above, the use of laser annealing might increase the Ni(GeSn) texture. This phenomenon yielded to better defined interfaces, which are assumed to decrease the intrinsic contact resistivity and thus be consistent with improved electrical performances [51]. If the high R_{sh} values for RTA processes were likely due to Ni(GeSn) agglomeration and Sn segregation phenomena [17], [24], the R_{sh} moderate increase seems, for UV-NLA, only to be due to the formation of wrinkles.

V. CONCLUSION

In summary, we considered the adoption of UV-nanosecond laser annealing (UV-NLA) to achieve more stable Ni(GeSn) alloys than with conventional rapid thermal annealing (RTA).

As far as the phase sequence was concerned, we had an overall evolution similar to that with RTA. At low laser energy densities (ED) and after the consumption of Ni, the Ni-rich $Ni_5(GeSn)_3$ phase was first obtained. This phase was followed, for higher ED, by the mono-stanogermanide phase Ni(GeSn). We did not observe any diffraction lines associated with the presence of Sn.

Wrinkles were formed at high ED. This phenomenon was likely due to some stress relaxation of the TiN capping layer when the melting threshold of the GeSn layer underneath was reached. The number and amplitude of wrinkles increase with the energy density and, for a given ED, the number of laser pulses. Cross-sectional observations indicated that the Ni(GeSn) composition was quite homogeneous without any evidence of Sn segregation or NiGe agglomeration.

The variation of sheet resistance (R_{sh}) values was mainly governed by the phases in presence at low energy density. At higher ED, morphological changes (mainly due to surface wrinkles) resulted in a R_{sh} increase. This increase was quite moderate compared to RTA. Thanks to UV-NLA, we also obtained a larger process window and slightly lower R_{sh} values.

We conclusively established that UV-NLA is a viable technique to obtain Ni-based contacts on GeSn. UV-NLA yielded thermally stable Ni(GeSn) without Sn segregation or NiGe agglomeration. Those features are promising in order to have high quality electrical contacts on GeSn devices.

ACKNOWLEDGMENT

The authors would like to express sincere thanks to Denis Mariolle and Nicolas Chevalier (CEA-Leti) for their assistance during AFM measurements. Part of this work was done on the NanoCharacterization PlatForm (PFNC) and was supported by the "Recherches Technologiques de Base" Program of the French Ministry of Research.

REFERENCES

[1] G. Han et al., "High-mobility germanium-tin (GeSn) P-channel MOSFETs featuring metallic source/drain and sub-370 °C process modules," in *Proc. Int. Electron Devices Meeting (IEDM)*, 2011, p. 16.
[2] Y. S. Huang et al., "Strained $Ge_{0.91}Sn_{0.09}$ quantum well p-MOSFETs," in *Proc. IEEE Silicon Nanoelectron. Workshop (SNW)*, 2016, pp. 132–133.
[3] S. Takeuchi et al., "$Ge_{1-x}Sn_x$ stressors for strained-Ge CMOS," *Solid-State Electron.*, vol. 60, no. 1, pp. 53–57, 2011.
[4] S. Wirths et al., "Ternary and quaternary Ni(Si)Ge(Sn) contact formation for highly strained Ge p- and n-MOSFETs," *Semicond. Sci. Technol.*, vol. 30, no. 5, 2015, Art. no. 55003.
[5] S. Wirths et al., "Lasing in direct-bandgap GeSn alloy grown on Si," *Nat. Photon.*, vol. 9, no. 2, pp. 88–92, 2015.
[6] V. Reboud et al., *Lasing in Group-IV Materials*. Cham, Switzerland: Springer,, 2021, pp. 105–195.
[7] C. Cardoux et al., "Direct band gap $Ge_{0.85}Sn_{0.15}$ photodiodes for room temperature gas sensing," in *Proc. IEEE Silicon Photon. Conf. (SiPhotonics)*, 2023, pp. 1–2.
[8] E. Talamas Simola et al., "CMOS-compatible bias-tunable dual-band detector based on GeSn/Ge/Si coupled photodiodes," *ACS Photon.*, vol. 8, no. 7, pp. 2166–2173, 2021.
[9] B. Marzban et al., "Strain engineered electrically pumped SiGeSn microring lasers on Si," *ACS Photon.*, vol. 10, no. 1, pp. 217–224, 2023.
[10] A. Bjelajac et al., "Up to 300 K lasing with GeSn-On-Insulator microdisk resonators," *Opt. Exp.*, vol. 30, no. 3, pp. 3954–3961, 2022.
[11] J. Chrétien et al., "Room temperature optically pumped GeSn microdisk lasers," *Appl. Phys. Lett.*, vol. 120, no. 5, 2022, Art. no. 51107.
[12] D. Buca et al., "Room temperature lasing in GeSn microdisks enabled by strain engineering," *Adv. Opt. Mater.*, vol. 10, no. 22, 2022, Art. no. 2201024.
[13] S. Wirths, D. Buca, and S. Mantl, "Si-Ge-Sn alloys: From growth to applications," *Prog. Cryst. Growth Charact. Mater.*, vol. 62, no. 1, pp. 1–39, 2016.
[14] I. S. Yu et al., "Investigation of $Ge_{1-x}Sn_x$/Ge with high Sn composition grown at low-temperature," *AIP Adv.*, vol. 1, no. 4, 2011, Art. no. 42118.
[15] F. A. Trumbore, "Solid solubilities and electrical properties of tin in germanium single crystals," *J. Electrochem. Soc.*, vol. 103, no. 11, p. 597, 1956.
[16] R. W. Olesinski and G. J. Abbaschian, "The Ge–Sn (germanium–tin) system," *Bull. Alloy Phase Diagr.*, vol. 5, no. 3, pp. 265–271, 1984.
[17] A. Quintero, P. Gergaud, J.-M. Hartmann, V. Reboud, and P. Rodriguez, "Ni-based metallization of GeSn layers: A review and recent advances," *Microelectron. Eng.*, vol. 269, Jan. 2023, Art. no. 111919.
[18] S. Wirths et al., "Ni(SiGeSn) metal contact formation on low bandgap strained (Si)Ge(Sn) semiconductors," *ECS Trans.*, vol. 64, no. 6, pp. 107–112, 2014.
[19] Y. Liu, H. Wang, J. Yan, and G. Han, "Reduction of formation temperature of nickel mono-stanogermanide [Ni(GeSn)] by the incorporation of tin," *ECS Solid State Lett.*, vol. 3, no. 2, pp. P11–P13, 2014.
[20] T. Nishimura et al., "Formation of $Ni(Ge_{1-x}Sn_x)$ layers with solid-phase reaction in $Ni/Ge_{1-x}Sn_x/Ge$ systems," *Solid-State Electron.*, vol. 60, no. 1, pp. 46–52, 2011.
[21] L. Wang et al., "Thermally stable multi-phase nickel-platinum stanogermanide contacts for germanium-tin channel MOSFETs," *Electrochem. Solid-State Lett.*, vol. 15, no. 6, pp. H179–H181, 2012.
[22] W. Wan et al., "Effect of platinum interlayer on the thermal stability improvement of nickel stanogermanide," in *Proc. 18th Int. Workshop Junct. Technol. (IWJT)*, 2018, pp. 1–3.
[23] A. Quintero et al., "Impact of Pt on the phase formation sequence, morphology and electrical properties of $Ni(Pt)/Ge_{0.9}Sn_{0.1}$ system during solid-state reaction," *J. Appl. Phys.*, vol. 124, no. 8, 2018, Art. no. 85305.
[24] A. Quintero, P. Gergaud, J.-M. Hartmann, V. Reboud, E. Cassan, and P. Rodriguez, "Impact of alloying elements (Co, Pt) on nickel stanogermanide formation," *Mater. Sci. Semicond. Process.*, vol. 108, Mar. 2020, Art. no. 104890.
[25] Q. Liu et al., "Improvement of the thermal stability of nickel stanogermanide by carbon pre-stanogermanidation implant into GeSn substrate," *ECS J. Solid State Sci. Technol.*, vol. 4, no. 3, pp. P67–P70, 2015.
[26] A. Quintero et al., "Enhanced thermal stability of Ni/GeSn system using pre-amorphization by implantation," *J. Appl. Phys.*, vol. 129, no. 11, 2021, Art. no. 115302.
[27] Y. Wu, H. Xu, K. Han, and X. Gong, "Thermal stability and Sn segregation of low-resistance Ti/p^+-$Ge_{0.95}Sn_{0.05}$ contact," *IEEE Electron Device Lett.*, vol. 40, no. 10, pp. 1575–1578, Oct. 2019.
[28] A. Quintero, P. Gergaud, J.-M. Hartmann, V. Reboud, E. Cassan, and P. Rodriguez, "Impact of Sn on the Ti/Ge solid-state reaction: Phase formation sequence, morphological and electrical properties," *Microelectron. Eng.*, vol. 252, Jan. 2022, Art. no. 111667.
[29] L. Wei et al., "Reaction of titanium-modulated nickel with germanium-tin under microwave and rapid thermal annealing," *Acta Physica Sinica*, vol. 70, no. 11, 2021, Art. no. 116801.
[30] E. Galluccio, G. Mirabelli, A. Harvey, M. Conroy, E. Napolitani, and R. Duffy, "Cell formation in stanogermanides using pulsed laser thermal anneal on $Ge_{0.91}Sn_{0.09}$," *Mater. Sci. Semicond. Process.*, vol. 121, Jan. 2021, Art. no. 105399.
[31] S. Abdi, S. Assali, M. R. M. Atalla, S. Koelling, J. M. Warrender, and O. Moutanabbir, "Recrystallization and interdiffusion processes in laser-annealed strain-relaxed metastable $Ge_{0.89}Sn_{0.11}$," *J. Appl. Phys.*, vol. 131, no. 10, 2022, Art. no. 105304.
[32] A. Quintero, P. A. Alba, J.-M. Hartmann, P. Gergaud, V. Reboud, and P. Rodriguez, "Innovative annealing technology for thermally stable Ni(GeSn) alloys," in *Proc. 21st Int. Workshop Junct. Technol. (IWJT)*, 2023, pp. 1–4.
[33] M. Kurosawa, N. Taoka, H. Ikenoue, O. Nakatsuka, and S. Zaima, "Large grain growth of Ge-rich $Ge_{1-x}Sn_x$ ($x \approx 0.02$) on insulating surfaces using pulsed laser annealing in flowing water," *Appl. Phys. Lett.*, vol. 104, no. 6, 2014, Art. no. 61901.
[34] R. Matsumura, H. Chikita, Y. Kai, T. Sadoh, H. Ikenoue, and M. Miyao, "Low-temperature (–180 °C) position-controlled lateral solid-phase crystallization of GeSn with laser-anneal seeding," *Appl. Phys. Lett.*, vol. 107, no. 26, 2015, Art. no. 262106.
[35] L. Zhang et al., "Poly-GeSn junctionless thin-film transistors on insulators fabricated at low temperatures via pulsed laser annealing," *Phys. Status Solidi Rapid Res. Lett.*, vol. 13, no. 11, 2019, Art. no. 1900420.
[36] L. Casiez et al., "Recrystallization of thick implanted GeSn layers with nanosecond laser annealing," *J. Appl. Phys.*, vol. 131, no. 15, 2022, Art. no. 153103.
[37] X. Wang et al., "Effect of laser pulse width and intensity distribution on the crystallographic characteristics of GeSn film," *Coatings*, vol. 13, no. 2, p. 453, 2023.
[38] P. Scajev et al., "Extension of spectral sensitivity of GeSn IR photodiode after laser annealing," *Appl. Surf. Sci.*, vol. 555, Jul. 2021, Art. no. 149711.
[39] J. Aubin, J. M. Hartmann, J. P. Barnes, J. B. Pin, and M. Bauer, "Very low temperature epitaxy of heavily in situ phosphorous doped Ge layers and high Sn content GeSn layers," *ECS J. Solid State Sci. Technol.*, vol. 6, no. 1, pp. P21–P26, 2017.
[40] A. Quintero, P. Gergaud, J. Aubin, J.-M. Hartmann, V. Reboud, and P. Rodriguez, "Ni/GeSn solid-state reaction monitored by combined X-ray diffraction analyses: Focus on the Ni-rich phase," *J. Appl. Cryst.*, vol. 51, no. 4, pp. 1133–1140, 2018.

[41] H. Khelidj, "Elaboration de films minces semi-conducteurs $Ge_{1-x}Sn_x$ et leurs contacts ohmiques," Ph.D. dissertation, IMMNP, Aix-Marseille Université, Marseille, France, 2021.

[42] H. Khelidj, A. Portavoce, K. Hoummada, M. Bertoglio, M. C. Benoudia, and D. Mangelinck, "Segregation kinetics of Sn in Ni(GeSn) phase," in *Proc. 30th Mater. Adv. Metallizat. (MAM-2022)*, 2022.

[43] J. Aubin et al., "Impact of thickness on the structural properties of high tin content GeSn layers," *J. Cryst. Growth*, vol. 473, pp. 20–27, Sep. 2017.

[44] I. Karmous et al., "Non-equilibrium growth of surface wrinkles emerging in an SiO_2/Si stack during Si melting induced by UV nanosecond pulsed laser annealing," *ECS J. Solid State Sci. Technol.*, vol. 11, Oct. 2022, Art. no. 104006.

[45] A. Quintero, P. Gergaud, J.-M. Hartmann, V. Reboud, E. Cassan, and P. Rodriguez, "Effects of alloying elements (Pt or Co) on nickel-based contact technology for GeSn layers," in *Proc. 19th Int. Workshop Junct. Technol. (IWJT)*, 2019, pp. 1–4.

[46] A. R. Shugurov, A. I. Kozelskaya, and A. V. Panin, "Wrinkling of the metal–polymer bilayer: The effect of periodical distribution of stresses and strains," *RSC Adv.*, vol. 4, p. 7389, Jan. 2014.

[47] A. Quintero et al., "Impact and behavior of Sn during the Ni/GeSn solid-state reaction," *J. Appl. Cryst.*, vol. 53, no. 3, pp. 605–613, 2020.

[48] A. Quintero et al., "Analysis of Sn behavior during Ni/GeSn solid-state reaction by correlated X-ray diffraction, atomic force microscopy, and ex-situ/in-situ transmission electron microscopy," *ECS Trans.*, vol. 98, no. 5, pp. 365–375, 2020.

[49] H. Marom and M. Eizenberg, "The effect of surface roughness on the resistivity increase in nanometric dimensions," *J. Appl. Phys.*, vol. 99, Jun. 2006, Art. no. 123705.

[50] S.-C. Teng, Z.-Y. Liang, C.-P. Chou, Y.-H. Tsai, P.-W. Chiu, and Y.-H. Wu, "Co silicide with low contact resistivity formed by atomic layer deposited cobalt and subsequent annealing," *IEEE Electron Device Lett.*, vol. 41, no. 1, pp. 139–142, Jan. 2020.

[51] C. Feautrier et al., "Impact of laser anneal on NiPt silicide texture and chemical composition," *J. Appl. Phys.*, vol. 121, no. 22, 2017, Art. no. 225109.